Indian Journal of Biochemistry & Biophysics
Vol. 62, July 2025, pp. 683-699
DOI: 10.56042/ijbb.v62i7.13656

Computational, Spectroscopic, Hirshfeld surface, Molecular docking and Topological studies on 2-bromo-5-methylpyridine as potent anti-cancer agent

J Senthil Kumar[1], N Siva Jyothi[2], S Sumathi[3], N Karthik[3] & S Jeyavijayan[3]*

[1]Department of Physics, Thanthai Periyar Government Arts and Science College, Tiruchirappalli-620 023, Tamil Nadu, India
[2]Department of Physics, Periyar Maniammai Institute of Science and Technology, Vallam, Thanjavur-613 403, Tamil Nadu, India
[3]Department of Physics, Kalasalingam Academy of Research and Education, Krishnankoil-626 126, Tamil Nadu, India

Received 10 September 2024; *revised 07 January 2025*

2-Bromo-5-methylpyridine (2BMP) has been found to show FTIR and FT-Raman spectra in the 3500-400 cm^{-1}. The density functional theory (DFT/B3LYP) method was applied to determine the structure, frequencies, Raman activities, and infrared intensities of the molecule using 6-311++G(d,p). The study of molecular orbital contributions has been done with the use of the DOS spectrum. Natural bond orbital (NBO) analysis has been used to calculate the stability of a molecule resulting from hyper-conjugative $\pi \rightarrow \pi^*$ exchanges and charge delocalisation. Furthermore, the 2BMP's Fukui function, Mulliken charges, and NMR chemical shifts have been examined. Thermodynamic, LOL, and ELF characteristics were investigated topologically in relation to temperature. The binding affinities of breast cancer inhibitors like 1ERE, 1AQU, and 4OAR are found as -5.1, -5.4, and -5.4 Kcal/mol from the docking study. Prescription medications and these affinities are similar. Through ADMET analysis, the degree of drug-likeness in a molecule has been investigated and evaluated.

Keywords: 2-bromo-5-methylpyridine, ADMET, Breast cancer, DFT, Docking

Heterocyclic derivatives containing nitrogen, including pyridine frameworks and azines, are essential compounds in chemistry and biology that are widely used in the production of vitamins, natural products, drugs, and functional reagents[1]. Pyridine derivatives are known to have better medicinal qualities. These unique characteristics have prompted researchers studying organic chemistry to focus more on crucial molecules with distinct geometries that characterize the target molecule's biological selectivity and suggest potential interactions with particular proteins or DNA[2]. The possible benefits of pyridine derivatives include anti-cancer[3], anti-bacterial[4], anti-fibrotic agents[5], anti-inflammatory[6], cardiotonic[7], IKK-β inhibitors[8], and HIV-1 inhibitor[9]. The molecular structure of pyridine derivatives has been the subject of recent computational and spectroscopic investigations by several researchers[10,11]. Cancer is now the main factor contributing to the growing worldwide death rate, with the potential to cause nearly 10 million fatalities yearly. There are several treatment options available, including as surgery, chemotherapy, and radiation. However, a few of these result in the loss of healthy cells, which may be lethal for the affected individuals. Thus, efforts to find ways to eliminate cancerous cells on a specific basis have continued[12]. DFT examines the structural and electronic excited state features of 2-bromo-5-methylpyridine (2BMP) that are related to its stability and reactivity[13]. The orbital energy, vibrational frequencies, and molecular geometry of a molecule may all be calculated using DFT. Additionally, it has been discovered that the functional B3LYP offers a remarkable trade-off between the vibrational spectrum ofmolecules[14].

One of the pyridine compounds, 2BMP, was chosen for the current investigation, and a comprehensive spectroscopic examination was performed. There are no reports of quantum chemical or vibrational analysis of 2BMP, according to a review of the literature. The basis set B3LYP/6-311++G(d,p) was used to analyse the molecule 2BMP. Initially, the Gaussian 09 program[15] was used to optimise the 2BMP's structure. The PED calculations[16] made by the VEDA 4.0 tool have been calculated and confirmed the harmonic vibrational wave numbers of 2BMP. The relationship between

*Correspondence:
E-mail: s.jeyavijayan@gmail.com

the experimentally acquired data and the NMR chemical shifts of 2BMP has been computed. It has been determined that 2BMP is reactive and kinetically stable using HOMO-LUMO analysis. The MEP surface analysis, Mullikan distribution computation, electronic absorbance data comparison in aqueous solution, and natural bond orbital (NBO) study, which verifies 2BMP's bioactivity, are utilised to ascertain the structure. To acquire a better understanding of 2BMP's inhibitory properties against several breast cancer proteins, a docking study was conducted. ADMET analysis of 2BMP has been investigated to determine its drug-likeness.

Experimental and characterization

Characterization techniques

The substance was allegedly 98% pure, and it was purchased from Sigma-Aldrich Corporation and used. The structural information of the molecule has been examined in the 2θ range of 10˚–50˚ using an X-ray diffractometer (BRUKER-D8). The FTIR was obtained in the range of 3500-400 cm^{-1} with polystyrene bands. Because the sample was in a solid condition, the KBr disc technique was used to produce it. FT-Raman could separate spectra at wave numbers of 3500-400 cm^{-1} at the chamber temperature. The UV-Vis spectrum between 100 to 400 nm in wavelength was measured using a UV-Vis (UV-2600) spectrophotometer. Using DMSO-d6 as the deuterated solvent, the ^{1}H and ^{13}C NMR of 2BMP were recorded using the Bruker 400 MHz Avance III HD Nanobay NMR spectrometer.

Computational details

Quantum chemistry computations of 2BMP were performed using the B3LYP/6-311++G(d,p) basis set[17]. Using the optimised molecular structure, the infrared intensity and Raman activity were calculated. Using VEDA software[16], vibrational assignments were assigned to 2BMP by PED. To get around this, the computed resonance frequencies have been modified using a scaling factor[18] of 0.9613. The Time-dependent DFT method has been used to determine electronic transitions, absorption, and vertical excitation energies. Hence, NBO calculations[19] have been carried. The GIAO approach uses optimal limits to simulate ^{13}C and ^{1}H NMR shifts. From these calculations, DOS spectra were generated using Gauss Sum 3.0 too[20]. A molecule's individual atom's charge can be estimated using Mulliken population analysis. The Multiwfn program was used to analyse RDG, ELF and LOL plots[21].

Molecular docking and ADMET prediction

Human progesterone and estrogen receptors cause several cellular downstream signalling pathways, which in turn cause cancer to form and spread. Utilising a computer-aided molecular modelling technique, we evaluated 2BMP's inhibitory efficacy against breast cancer. Protein markers for breast cancer include the human progesterone (PDB ID: 4OAR), human estrogen (PDB ID: 1ERE) receptor, and estrogen sulfotransferase (PDB ID: 1AQU) receptor. These receptors are used as protein indicators, and the chemical 2BMP as a ligand. PyMOL molecular graphical system[22] and Auto Dock Vina[23]were used to display the protein-ligand binding position. Using Discovery Studio[24], the protein structure and amino acid locations were examined. Using the pkCSM server[25], the pharmacokinetic and physicochemical characteristics of the medicinal compound 2BMP were ascertained. These qualities included absorption, metabolism, excretion, and toxicity. The BOILED-Egg model was then run on the Swiss-ADME web server[26], and a variety of pharmacokinetic features, including drug similarity and water solubility, were predicted.

Result and Discussion

Molecular geometry analysis

According to XRD data[27], 2BMP crystallizes in the monoclinic space group P21/m with the unit cell parameters of a = 6.1889 (18) Å, b = 6.614 (2) Å, c = 7.835 (2) Å, β = 93.503 (9)˚, V=320.12 (17) Å3 and Z = 2. The powder XRD pattern of the crystal formed from the standard Crystallographic Information File (CIF) is displayed in (Fig. 1), along with the 2BMP powder X-ray diffraction pattern that was obtained. Both the XRD patterns of 2BMP have been well correlated each other and the structure of the sample was confirmed by this pattern. For the molecular structure of 2BMP, the C_1 point group exhibits symmetry. The optimised structural parameters are calculated at the DFT-B3LYP level using the 6-311++G(d,p) basis set, in accordance with the atom numbering system depicted in (Fig. 2). In this study, we have compared the experimental values[27] of the molecule with the theoretical values given in (Table 1). Table 1 displays the results of an RMSD (Root Mean Square Deviation) computation that was performed to compare the experimental and theoretical data in order to evaluate how well the theoretical model fits reality (R^2 = 0.982 for bond lengths and R^2 = 0.954 for bond angles).

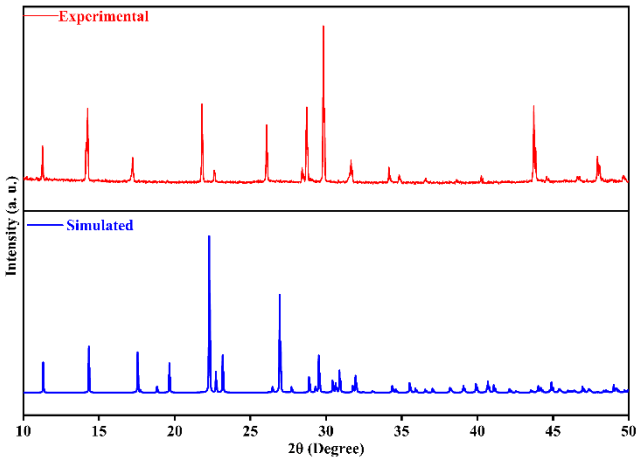

Fig. 1 — Simulated XRD of 2-bromo-5-methylpyridine compared with experimental X-ray diffraction pattern

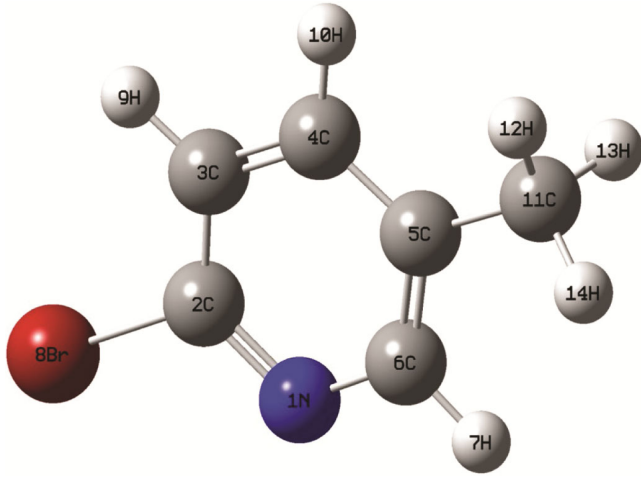

Fig. 2 — Optimized structure of 2-bromo-5-methylpyridine

This molecule is composed of one C-Br bond, two C-N bond, five C-C bonds, and six C-H bonds. It has been demonstrated that C-H bond lengths for 2BMP vary from 1.08 to 1.09 Å. Using the B3LYP/6-311++G (d,p) method, the C-C bond distances are elevated from 1.34 to 1.51 Å, are compared in the XRD values (1.34-1.50Å). From the bond angles for C2-C1-C6, C3-C2-Br8, and C4-C3-H9, is determined to be 117.63°, 118.61°, and 121.79° (corresponding experimental values: 116.10°, 118.80°, and 120.00°). The calculated and experimental parameters correlate well, as evidenced by the correlation coefficient plot as shown in (Fig. 3). Utilizing the DFT/B3LYP and 6-311++G(d,p) methodologies, the thermodynamic properties of 2BMP were investigated. Table 2 presents the findings. The molecule 2BMP has a greater dipole moment of 4.08 Debye because of the highly electronegative nitrogen and bromine atoms and their charges. It is discovered that 2BMP has an

Table 1 — The optimized structural parameters of 2-bromo-5-methylpyridine

Structural parameters		
Bond length (Å)	DFT-B3LYP/6-311++G(d,p)	Experimental [27] $R^2 = 0.982$
C1-C6	1.34	1.34
C2-C3	1.40	1.38
C2-Br8	1.93	1.92
C3-C4	1.39	1.38
C3-H9	1.08	0.95
C4-C5	1.40	1.40
C4-H10	1.09	0.95
C5-C6	1.39	1.39
C5-C11	1.51	1.50
C6-H7	1.09	0.95
C11-H12	1.09	0.95
C11-H13	1.09	0.95
C11-H14	1.09	0.95
Bond angle (°) $R^2 = 0.954$		
C2-C1-C6	117.63	116.10
C1-C2-C3	124.42	125.80
C1-C2-Br8	116.97	115.50
C3-C2-Br8	118.61	118.80
C2-C3-C4	117.12	117.00
C2-C3-H9	121.08	121.50
C4-C3-H9	121.79	120.00
C3-C4-C5	120.25	120.00
C3-C4-H10	119.60	120.00
C5-C4-H10	120.15	120.00
C4-C5-C6	116.50	116.90
C4-C5-C11	121.94	121.60
C6-C5-C11	121.56	121.50
C1-C6-C5	124.09	124.30
C1-C6-H7	115.59	117.90
C5-C6-H7	120.32	117.80
C5-C11-H12	111.22	111.30
C5-C11-H13	111.22	111.30
C5-C11-H14	111.17	111.30
H12-C11-H13	107.38	109.10
H12-C11-H14	107.84	109.10
H13-C11-H14	107.84	109.10

overall energy of 70.81 Kcal mol^{-1} and entropy of 88.24 cal $mol^{-1}K^{-1}$. At 66.13 Kcal mol^{-1}, the immaterial vibrational energy (zero-point) for 2BMP is reached. The chemical reactions of 2BMP may be assessed using these thermodynamic properties.

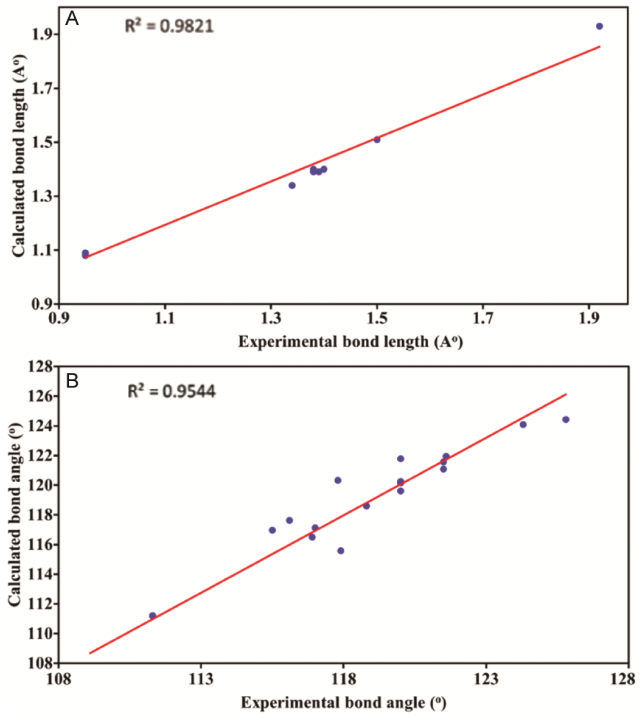

Fig. 3 — Correlation graphs of the calculated and experimental molecule (A) bond distances; and (B) bond angles of 2-bromo-5-methylpyridine

Vibrational analysis

The modes of 2BMP, which are active in the infrared and Raman spectra, are controlled by its 14 atoms. The experimental and computational spectra of 2BMP are shown in (Fig. 4). Table 3 contains the fundamental modes of 2BMP. The primary goal of this study is to properly assign the experimental frequencies to the various vibrational modes of 2BMP in concordance with the harmonic vibrational frequencies estimated at the DFT. The overestimation of the predicted vibrational modes is a result of the real system's lack of anharmonicity, as demonstrated by a comparison between the experimental results and

Table 2 — The thermodynamic parameters of 2-bromo-5-methylpyridine

Parameters	DFT-B3LYP/ 6-311++G(d,p)
Optimized global minimum Energy (Hartrees)	-2861.22428613
Total energy(thermal), E_{total} (kcal mol^{-1})	70.81
Heat capacity, C_v (cal mol^{-1} k^{-1})	26.65
Total Entropy, S (cal mol^{-1} k^{-1})	88.24
Translational Entropy (cal mol^{-1} k^{-1})	41.32
Rotational Entropy (cal mol^{-1} k^{-1})	29.39
Vibrational Entropy (cal mol^{-1} k^{-1})	17.53
Vibrational energy, E_{vib} (kcal mol^{-1})	69.03
Zero-point vibrational energy, (kcal mol^{-1})	66.13
Rotational constants (GHz)	
A	5.73
B	0.65
C	0.58
Dipole moment (Debye)	4.08

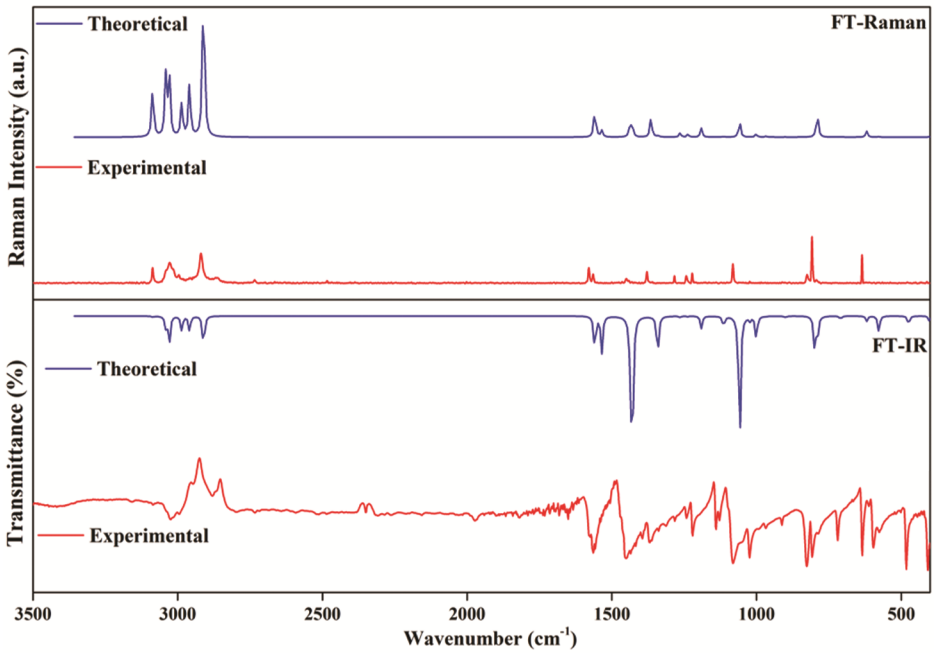

Fig. 4 — FT-IR and FT-Raman spectra of 2-bromo-5-methylpyridine

Table 3 — The vibrational assignments based on PED calculations for 2-bromo-5-methylpyridine

S. No	Observed wave number (cm^{-1})		Wavenumber (cm^{-1})		IR Intensity (Km mol^{-1})	Raman activity ($Å^4$ amu^{-1})	Assignment with PED (%)
	FT-IR	FT- Raman	Calculated	Scaled			
1	-	3085(ms)	3211	3087	0.86	99.36	νCH(100)
2	-	3042(s)	3164	3041	9.06	107.43	νCH(99)
3	3028(w)	3028(vw)	3152	3030	23.38	114.05	νCH(96)
4		2914(s)	3107	2986	12.88	63.13	CH_3ips(95)
5	2963(vw)	-	3078	2959	13.23	100.62	CH_3ss(94)
6	2885(w)	2857(vw)	3028	2911	27.37	289.85	CH_3ops(93)
7	1557(ms)	1585(w)	1621	1559	29.15	34.25	νCC(91)
8	1520(ms)	1542(vw)	1597	1535	30.82	7.99	νCC(90)
9	-	1457(w)	1495	1437	18.95	13.19	CH_3ipb(88)
10	1425(ms)	-	1488	1430	127.04	4.38	νCC(86)
11	-	-	1487	1430	8.29	10.13	νCC(83)
12	-	1310(vw)	1420	1365	0.29	22.46	νCC(84)
13	1345(ms)	-	1396	1342	36.20	1.64	CH_3sb(85)
14	1257(w)	1230(vw)	1315	1265	1.07	4.54	νCN(82)
15	1228(vw)	-	1287	1237	0.45	2.95	νCN(81)
16		1165(w)	1239	1191	10.12	10.02	CH_3opb(80)
17		1085 (w)	1159	1114	9.15	0.53	bCH(78)
18	1071(ms)	-	1101	1058	112.42	17.36	bCH(79)
19	-	1054 (w)	1064	1023	3.44	0.20	bCH(76)
20	1014(ms)	-	1041	1001	19.30	3.11	CH_3ipr(74)
21	-	-	1006	967	0.22	1.04	ωCH(72)
22	-	-	984	945	0.06	0.05	ωCH(71)
23	-	-	936	900	1.18	0.11	ωCH(75)
24	800(ms)	-	832	799	26.80	0.43	CH_3opr(74)
25	750(vw)	785(vs)	822	790	18.77	24.67	νCBr(73)
26	628(vw)	-	738	710	2.39	0.28	bCC(77)
27	614(w)	642(s)	644	619	4.21	5.86	Rasymd(68)
28	571(vw)	-	601	578	12.99	0.44	Rsymd(67)
29	-	-	494	475	7.82	0.13	Rtrigd(69)
30	420(ms)	-	420	404	3.88	0.28	ωCC(65)
31	-	-	366	352	1.16	0.96	tRasymd(64)
32	-	-	297	285	0.18	1.74	tRsymd(62)
33	-	-	286	275	6.30	10.17	`tRtrigd(61)
34	-	-	216	208	0.78	0.11	bCBr(59)
35	-	-	102	98	0.50	0.06	ωCBr(57)
36	-	-	65	62	0.08	0.65	tCH_3 (58)

the frequencies determined using the DFT-B3LYP approach[17].

CH_3 group vibrations

A total of nine fundamentals should be assigned frequencies to each CH_3 group: the CH_3 symmetrical stretching, the CH_3 in-plane stretching, the CH_3 out-of-plane stretching, the CH_3 in-plane bending, the symmetrical deformation modes, asymmetrical deformation modes, the in-plane rocking, the out-of-plane rocking, and twisting t(CH_3) modes. The detection ranges for asymmetric and symmetric stretching vibrations are 3010-2970 and 2940-2900 cm^{-1}, respectively. The FTIR and Raman spectra of 2BMP show that its CH_3 symmetric and in-plane stretching frequencies are located at 2963 cm^{-1} and 2914 cm^{-1}, respectively. The CH_3 symmetric bending at 1345 cm^{-1} and the CH_3 in-plane bending modes at 1457 cm^{-1} are identified in the spectra. In the infrared, the in-plane and out-of-plane rocking modes of CH_3 are responsible for the bands seen at 1014 cm^{-1} and 800 cm^{-1}. The CH_3 out-of-plane stretching and bending modes are found at 2885, 2857, and 1165 cm^{-1} in the infrared and Raman spectra, respectively. Table 3 presents the remaining modes of vibration of the CH_3 group. These modes likewise exhibit strong agreement with the assignments and get support from the reported literature[28].

C-H vibrations

Many weak bands that are commonly seen in the 3100–3000 cm^{-1} region of aromatic compounds are caused by the C–H stretching vibrations[29]. As a result, C-H stretching vibrations have been identified at 3085, 3042, and 3028 cm^{-1} in Raman as well as the IR

band at 3028 cm^{-1}. Their PED values confirm this identification. Sharp bands that interact with C-C stretching vibrations are seen in the 1300-1000 cm^{-1} area and are linked to C-H in-plane ring bending vibrations. In 2BMP, the vibrational bands at 1085, 1071, and 1054 cm^{-1} are indicative of the C–H in-plane bending vibrations. The C-H's highly coupled out-of-plane bending vibrations are located between 900 and 667 cm^{-1}. Excellent agreement is found between the theoretically expected values for C-H vibrational modes via the B3LYP/6-311++G(d,p) method and the observed results.

Pyridine ring vibrations

The C-C stretching ring of pyridine and the C-N stretching bands of aromatic rings are often identified within the respective frequency[19] ranges of 1600-1450 cm^{-1} and 1450-950 cm^{-1}. The C-N stretching modes, which are calculated as 1265, 1237 cm^{-1} using the B3LYP/6-311++G(d,p) method, are assigned to the experimental wave numbers 1257, 1228 cm^{-1} in FTIR and 1230 cm^{-1} in FT-Raman. The location and mass of the vibrational mode are significant determinants in pyridine ring breathing, which typically occurs in the wave number range of 900–750 cm^{-1}. The ring vibrational modes of 2BMP are identified by the wave numbers in the FT-IR at 614 and 571 cm^{-1}, as well as the FT-Raman spectrum at 642 cm^{-1}. Table 3 illustrates the observed skeleton vibrational modes and ring out-of-plane vibrations, which exhibit a strong connection with the experimental findings.

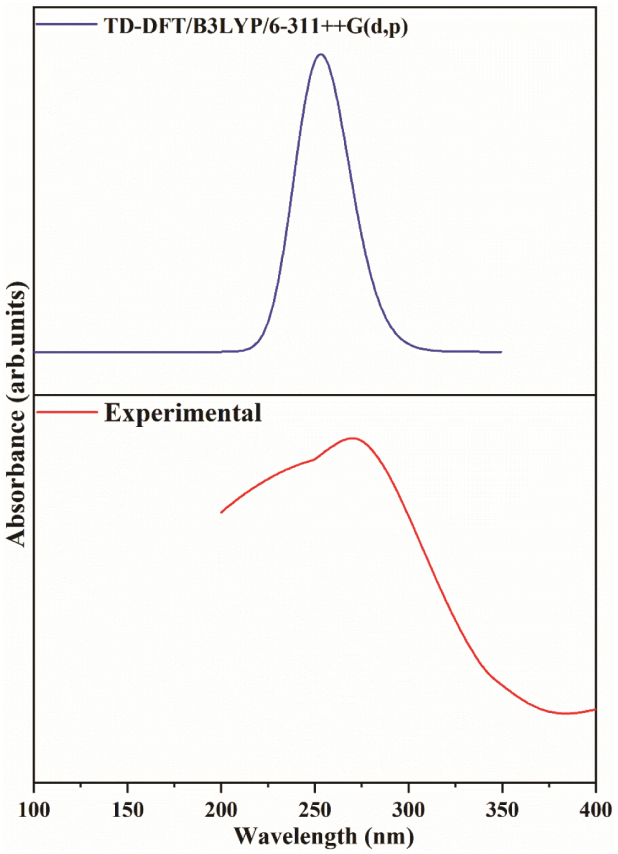

Fig. 5 — UV-Vis spectra of 2-bromo-5-methylpyridine

C–Br vibrations

The most aromatic bromo compounds[19] (C-Br stretching vibrations) occur in the range of 650 to 395 cm^{-1}. Due to the possibility of a combination of vibrations caused by the heavy atoms, the vibration linked to the bromine atom and ring is the most prominent. The current investigation has detected C-Br vibration at 750 cm^{-1} in FTIR and 785 cm^{-1} in FT-Raman. The in-plane and out-of-plane C-Br vibrations for 2BMP are measured at 208 and 98 cm^{-1}, respectively, and are displayed in (Table 3).

UV-Vis Analysis

Time-dependent density functional theory has been used to study the molecular system's absorption characteristics (TD-DFT). Using the B3LYP/6-311++G(d,p) basis set, the electronic absorption spectrum of 2BMP was simulated using TD-DFT in the gas phase. Figure 5 displays the UV-Vis spectra of 2BMP. Absorption peaks at 271.22 nm in the experimental spectrum belong to the π to π* range and demonstrate a transition from HOMO to LUMO (90.34% contribution). The computed absorption wavelength, oscillator strength, and excitation energies[30] are displayed in (Table 4). The absorption peaks at 253.36 nm with excitation energies of 4.8936 eV, respectively, are visible in the computed spectra.

Frontier Molecular Orbitals (FMOs)

The chemical reactivity, electronic properties, and molecular transitions of the molecule may all be ascertained using the FMO analysis. Furthermore,

Table 4 — Molecular orbital contributions of 2-bromo-5-methylpyridine

TD-DFT/ B3LYP/6-311++G(d,p)					Experimental wavelength (nm)
Energy (eV)	Oscillator strength	Computed wavelength (nm)	Major contributions	Assignment	
4.8936	0.0592	253.36	H→L (90.34%)	π→π*	271.22

FMO analysis may be used to determine the properties of ligand molecules and their interactions with biological receptors[31]. The highest occupied molecular orbital (HOMO) and lowest unoccupied molecular orbital (LUMO), respectively, stand for the capacity to donate an electron to an empty orbital. E_{HOMO} of -7.02 eV and E_{LUMO} of -1.44 eV were discovered for the 2BMP molecule. The FMOs of 2BMP are shown in (Fig. 6). The main position of the HOMO was the bromine atom, while the main site of the LUMO was the pyridine ring moiety. FMOs are shown in red and green, respectively, for their positive and negative phases. The energy gap value of 5.58 eV for the 2BMP molecule was calculated in this case, suggesting that the molecule has a stable structure. LUMO energy and HOMO energy are associated with the ionization potential and electron affinity, respectively. Additionally, Table 5 presents the molecular characteristics of 2BMP linked to the FMOs, ascertained by employing Koopmans' theorem[32]. Electrophilicity index, ionization potential, electron affinity, hardness, chemical potential, and softness values are a few of these characteristics. A molecule's electronegativity (φ) indicates its ability to attract electrons. A stronger electron attraction is produced by a higher electronegativity value. The value of (φ) in 2BMP was found to be 4.23 eV. Softness (S) is the inverse of hardness (η), which represents the level of chemical reactivity. 2BMP's hardness and softness are determined to be 2.79 eV and 0.18 eV^{-1}, respectively. The electrophilicity (ω) scale developed by Domingo *et al.*[33] may be used to categorize organic compounds as minimal electrophiles (ω < 0.8 eV), medium electrophiles (0.8 < ω < 1.5 eV), or high electrophiles (ω > 1.5 eV). The 2BMP electrophilicity index (ω) in the gas phase is found to be 3.21 eV, indicating a strong electrophile.

In a border zone, adjacent orbitals may have comparable degenerate energy levels. If so, characterizing border orbitals only in terms of HOMO and LUMO may not be adequate. The density of states

Table 5 — Global reactivity descriptors for 2-bromo-5-methylpyridine

Molecular Properties	B3LYP/6-311++G(d,p)
HOMO (eV)	-7.02
LUMO (eV)	-1.44
ΔE (E_{HOMO} -E_{LUMO}) (eV)	5.58
Ionization potential (I) (eV)	7.02
Electron affinity (A) (eV)	1.44
Global hardness (η) (eV)	2.79
Global softness (S) (eV^{-1})	0.18
Electronegativity (χ) (eV)	4.23
Chemical potential (μ) (eV)	-4.23
Global electrophilicity (ω) (eV)	3.21

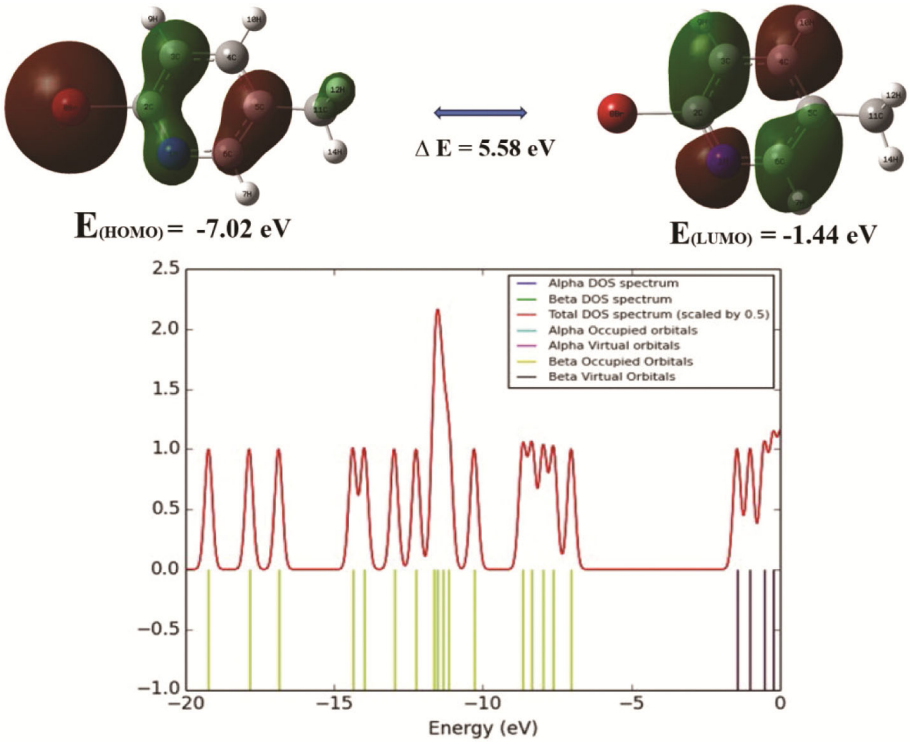

Fig. 6 — HOMO-LUMO and DOS spectrum of 2-bromo-5-methylpyridine

(DOS) is the total of the beta (β) and alpha (α) electron density of states since the molecular orbital information and Gaussian curves are merged using the Gauss Sum 3.0 program. The 42α and 42β combinations together make up the 84 electrons that occupy the DOS in 2BMP. As seen in Figure 6, the orbital structure of a molecule controls the chance of the chemical bonds that hold its atoms together.

Molecular electrostatic potential

MEP illuminates the responsive areas[34] of the chemical bonding process by utilizing its different colour codes. The MEP surfaces of 2BMP in the gas phase, computed at B3LYP/6-311++G(d,p), are displayed in (Fig. 7). The MEP increases our understanding in electrophilic, substituent effects, and inter-intramolecular interactions by establishing connections with the chemically active regions of molecules. Red, yellow, blue, and green have progressively stronger electrostatic potentials. The lone pair of nitrogen and bromine atoms in 2BMP form the electron-rich (red) and moderately electron-rich (yellow) portions. The electron-deficient (blue) portion of the molecule is surrounded by hydrogen atoms. The reason for this is because hydrogen atoms have joined the negatively charged nitrogen atoms. The ring system has the neutral electric potentials (green) surrounding it. It was anticipated that the electrophilic region of 2BMP would be found in the hydrogen atoms of the pyridine ring.

The most promising red regions in this analysis sufficiently illustrate the electrophilic character of nitrogen (N1). The other nitrogen (N1) shows some electrophilicity because of its link with a hydrogen atom. Every hydrogen possesses clusters of nucleophilic patches, with the hydrogen (H14) that is bonded to bromo having the most (blue area). The Mulliken charges map in Figure 8, which shows that atom C11, has the largest negative charge in comparison to atom C5 and atom H9 has the highest positive charge in comparison to other hydrogens in 2BMP, further supports this conclusion.

Natural bond orbital analysis

The NBO technique of provides the most realistic description of a "natural Lewis structure" because it mathematically modifies all orbital parameters. The NBO method's ability to produce information on interactions in both virtual and filled orbital spaces is a helpful feature that might improve research on intra- and intermolecular interactions[31]. The energy of electron transference or hyperconjugativecontact has been computed using the second-order perturbation method. The NBO study of 2BMP has evaluated the donor-acceptor interactions using the second-orderFock matrix by employing the B3LYP technique and the 6-311++G(d,p) basis set. The delocalization of electron density between occupied Lewis-type NBO orbitals and formally empty non-Lewis NBO orbitals can be used to represent a stabilizing donor-acceptor interaction. Table 6 provides a list of the corresponding outcomes. The orbitals interactions π(N1-C2)→π*(C5-C6), π(C5-C6)→π*(C3-C4), and π(C3-C4)→π*(N1-C2) in 2BMP have the greatest stabilization energies (10.63, 10.87, and 13.26 Kcal mol^{-1}). These interactions result in high electron concentrations in the anti-bonding C-C acceptor orbitals (about 0.877e, 0.818e, and 0.835e). Out of all antibonding orbitals, 69.06 and 49.44 Kcal mol^{-1} stabilize π*(N1-C2) → π*(C3-C4) and π*(N1-C2) → π*(C5-C6). Furthermore, the lone pairs bromine (Br8) provide transfer charges with magnitudes of 5.72 Kcal mol^{-1} to the antibonding

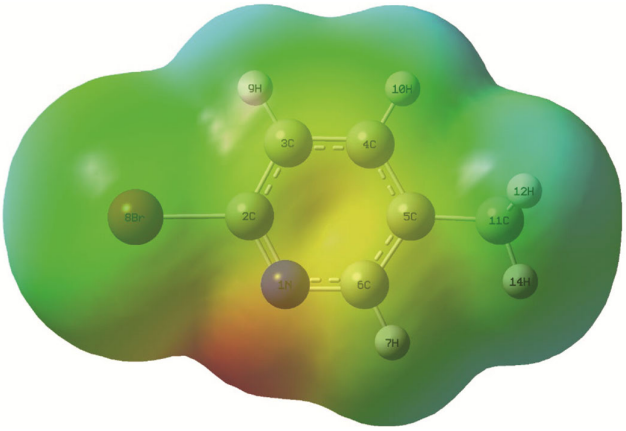

Fig. 7 — MEP plot over the atoms of 2-bromo-5-methylpyridine

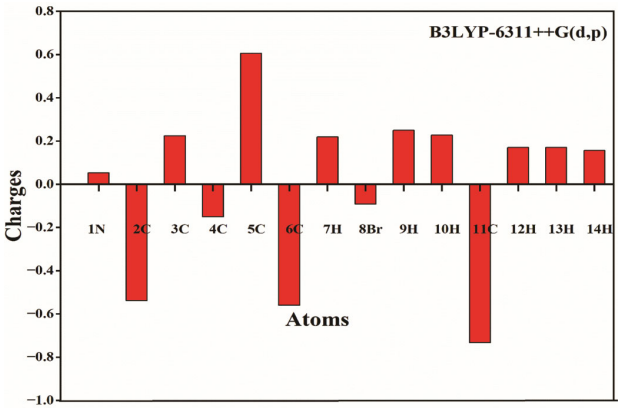

Fig. 8 — Mulliken population analysis of 2-bromo-5-methylpyridine

Table 6 — Second-order perturbation theory analysis of Fock matrix for 2-bromo-5-methylpyridine

Donor(i)	ED (i) (e)	Acceptor (j)	ED (j) (e)	Stabilization energy E(2) (Kcal/mol)	Energy difference E (j) −E (i) (arb. units)	Fock matrix element F(i,j) (arb. units)
π(N1-C2)	0.877	π*C3-C4	0.144	6.19	0.34	0.058
π(N1-C2)	0.877	π*C5-C6	0.150	10.63	0.35	0.078
σ(N1-C6)	0.986	σ*(C2-Br8)	0.035	2.94	0.91	0.066
σ(C3-C4)	0.985	σ*(C2-Br8)	0.035	2.64	0.8	0.059
π(C3-C4)	0.835	π*(N1-C2)	0.211	13.26	0.26	0.076
π(C3-C4)	0.835	π*(C5-C6)	0.150	8.93	0.29	0.065
σ(C3-H9)	0.990	σ*(N1-C2)	0.014	2.56	1.09	0.067
π(C5-C6)	0.818	π*(N1-C2)	0.211	9.45	0.26	0.063
π(C5-C6)	0.818	π*(C3-C4)	0.144	10.87	0.28	0.071
σ(C6-H7)	0.991	σ*(N1-C2)	0.014	2.21	1.08	0.062
σ(C6-H7)	0.991	σ*(C4-C5)	0.012	2.08	1.09	0.06
σ(C11-H14)	0.994	σ*(C4-C5)	0.012	2.34	1.07	0.063
LP(1)N1	0.946	σ*(C2-C3)	0.018	5.19	0.89	0.087
LP(1)N1	0.946	σ*(C2-Br8)	0.035	2.55	0.42	0.042
LP(1)N1	0.946	σ*(C5-C6)	0.016	4.19	0.91	0.079
LP(1)N1	0.946	σ*(C6-H7)	0.012	2.09	0.76	0.051
LP(2)Br8	0.987	σ*(N1-C2)	0.014	2.41	0.84	0.057
LP(3)Br8	0.966	π*(N1-C2)	0.211	5.72	0.28	0.055
π*(N1-C2)	0.211	π*(C3-C4)	0.144	69.06	0.02	0.084
π*(N1-C2)	0.211	π*(C5-C6)	0.150	49.44	0.03	0.081

π*(N1–C2) orbital. Strong hyperconjugative interactions between the nitrogen and bromine atoms and the ring structure result in a significant reduction of the lone pair electron density in comparison to other orbitals. Furthermore, the results from the HOMO-LUMO plot in the figure also generally mirror the results of NBO, as the bromine atom was the principal site for the HOMO and the pyridine ring moiety constituted the primary position for the LUMO.

Mulliken analysis

Mulliken populations provide one of the simplest representations of charge distribution[35]. We look at the atomic charges for 2BMP, which are displayed in (Fig. 8 and Table 7). In this case, the charges of the nitrogen (N1) atom are positive (0.053). The molecule is strongly acidic, as indicated by the optimistic hydrogen atoms of charges 0.219, 0.25, 0.227, 0.170, and 0.156 for 2BMP. The carbon atoms C3 and C5, which have respective positive charges of 0.224 and 0.606, are the strongest. The donor bromine atom (Br8) in the 2BMP has a negative charge of -0.092, while the most negatively charged atoms are C2, C4, C6, and C11 (-0.539, -0.151, -0.56, and -0.733). Substitutes have a major impact on the charges of both positive and negative carbon atoms.

Table 7 —Mulliken atomic charges for 2-bromo-5-methylpyridine

Atoms	Atomic Charges (Mulliken) by B3LYP/6-311++G(d,p)
N1	0.053
C2	-0.539
C3	0.224
C4	-0.151
C5	0.606
C6	-0.56
H7	0.219
Br8	-0.092
H9	0.25
H10	0.227
C11	-0.733
H12	0.17
H13	0.17
H14	0.156

Fukui function

Fukui function analysis is essential for understanding chemical reactivity and selectivity. Stated differently, it illustrates how the electron density may shift at a given site in order to provide or take up electrons that are more susceptible to assault by electrophiles or nucleophiles. Fukui functions have been determined for 2BMP for assaults that include electrophilic, radical, and

Table 8 — Fukui functions for 2-bromo-5-methylpyridine

Atoms	Mulliken Charges			Fukui functions			
	q(N+1)	q(N)	q(N-1)	f_k^+	f_k^-	f_k^0	$\Delta f(r)$
N1	-0.34	0.05	0.22	-0.39	-0.16	-0.28	-0.23
C2	1.80	-0.54	-0.54	2.34	0.00	1.17	2.34
C3	-1.11	0.22	0.29	-1.33	-0.07	-0.70	-1.27
C4	-0.69	-0.15	-0.09	-0.53	-0.06	-0.30	-0.47
C5	-0.19	0.61	0.59	-0.80	0.02	-0.39	-0.82
C6	-0.29	-0.56	-0.52	0.27	-0.04	0.11	0.31
H7	-0.55	0.22	0.27	-0.77	-0.05	-0.41	-0.72
Br8	0.54	-0.09	0.29	0.63	-0.38	0.13	1.01
H9	0.19	0.25	0.29	-0.06	-0.04	-0.05	-0.02
H10	-0.34	0.23	0.26	-0.57	-0.03	-0.30	-0.53
C11	-0.01	-0.73	-0.68	0.72	-0.06	0.33	0.78
H12	0.37	0.17	0.22	0.20	-0.05	0.08	0.25
H13	-0.27	0.17	0.22	-0.44	-0.05	-0.24	-0.39
H14	-0.16	0.16	0.18	-0.32	-0.03	-0.17	-0.29

nucleophilic attacks. It is possible to derive the Fukui function from each individual atomic charge by using Mulliken population analysis. A common method for calculating Fukui function[36] is:

$$f_k^+ = q_j(N+1) - q_j(N)$$

$$f_k^- = q_j(N) - q_j(N-1)$$

$$f_k^0 = \frac{1}{2}[q_j(N+1) - q_j(N-1)]$$

These groups are present in 2BMP and are free radical, electrophilic, and nucleophilic. The atom charge at the j^{th} position in the anionic (N+1) and cationic (N-1) chemical types is denoted by the symbol q_j. Morell *et al.*[37] recently presented a dual descriptor. Equation supports its definition, which states that it is the distinction between the electrophilic and nucleophilicfunctions:

$$\Delta f(r) = f_k^+ - f_k^-$$

Based on their sign, the dual descriptor differentiates between electrophilic and nucleophilic assaults at a certain location. Based on the values shown in Table 8, the nucleophilic sites for 2BMP are C2, C6, Br8, C11, and H12, which satisfy the dual descriptor criteria. In contrast, there are negative values for the electrophilic sites N1, C3, C4, C5, H7, H9, H10, H13, and H14. Depending on its local behaviour, the molecule 2BMP reacts to both electrophilic and nucleophilicattacks during the process.

NMR analysis

A more thorough discussion of 2BMP's characteristics is provided through ^{1}H and ^{13}C NMR spectroscopy. Using dimethyl-sulfoxide medium the NMR spectra of 2BMP are obtained. Gauge-independent atomic orbital technique (GIAO) was utilized to determine the ^{1}H and ^{13}C chemical shift values using the B3LYP method with 6-311++G(d,p) basis set. Table 9 presents the ^{13}C and H^1 chemical shifts of 2BMP that have been measured and estimated, using tetramethylsilane (TMS) as a reference. The data's spectral representation is displayed in (Fig. 9).

Table 9 — ^{13}C and ^{1}H NMR chemical shifts for 2-bromo-5-methylpyridine

Atoms	Experimental Shift (ppm)	Calculated shift (ppm) R^2=0.999
C11	-	17.62
C3	133.40	131.74
C5	138.77	137.13
C4	140.44	141.96
C6	150.90	154.61
C2	-	166.54
H14	-	1.98
H13	2.23	2.26
H12	2.23	2.26
H9	7.45	7.31
H110	7.48	7.40
H7	8.20	8.26

Ring carbon atom chemical changes usually fall between 100 and 200 ppm[30]. It is predicted that the ^{13}C NMR shift for C2 will be largest when nitrogen and bromine (N1 and Br8) provide the least effective shield. C2's calculated shift is 166.54 ppm. The carbon atom C11 connected with the ring system shows a little chemical change at 17.62 ppm as a result of the enhanced shielding effect. A greater wave number is obtained by direct connections or closeness to an electron-accepting atom, which reduces hydrogen shielding and enhances resonance.

Figure 9 shows that the predicted shift for H7, which is associated with the carbon atom (C6), exhibits a high value of 8.26 ppm. H7 exhibits a measured chemical change of 8.20 ppm in its ^{1}H NMR spectra. As hydrogens approach an electron donor, shielding increases and the resonance shifts to a shorter wavelength. As a result, the calculated shift for H14 produces a 1.98 ppm lower value.

Topological studies

Strong relationships between the structure and its surroundings, such as well-known H-bond partners, repulsive steric and Van der Waals forces, have been found using the Non-covalent interaction (NCI)[38]. The components of 2BMP configuration that demonstrate molecular docking, self-assembly, chemical firmness, biologic affinity and disinclination, and

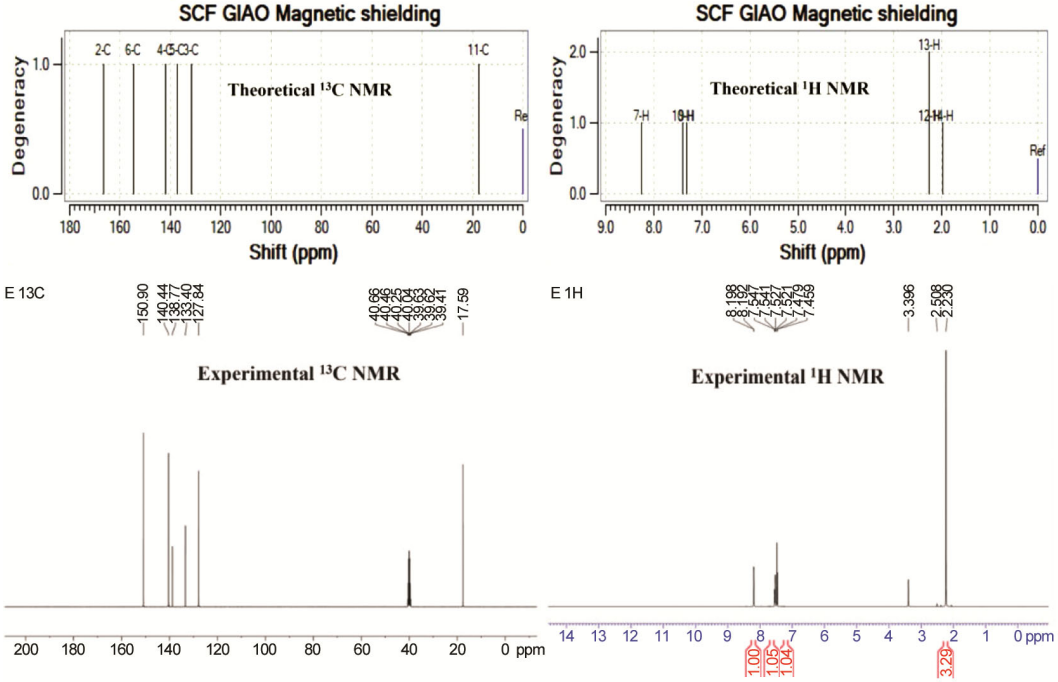

Fig. 9 — ^{13}C and ^{1}H NMR of 2-bromo-5-methylpyridine

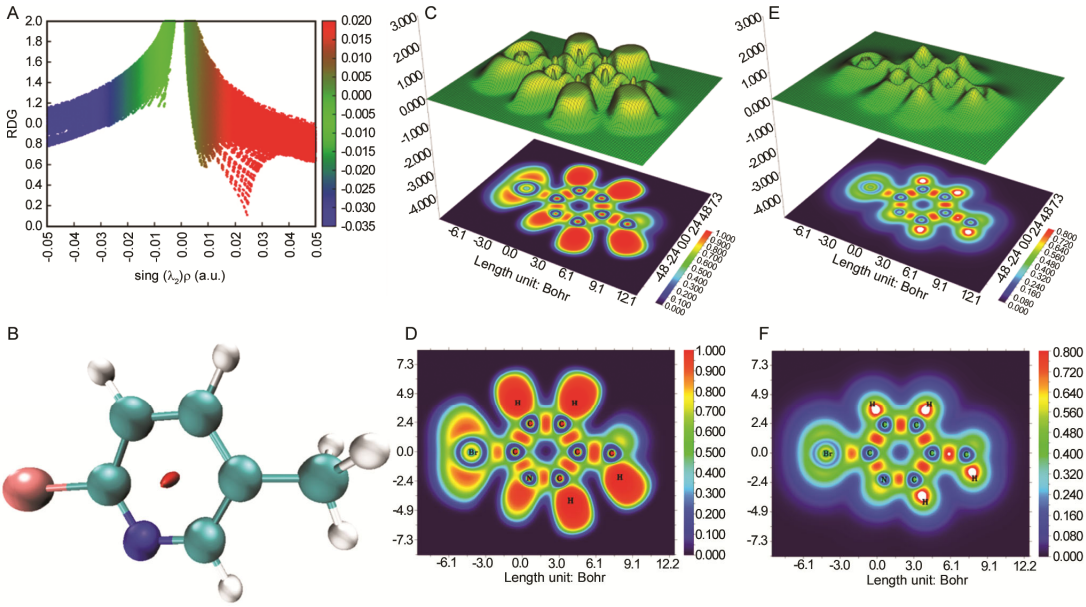

Fig. 10 — Representation of the outcomes of topological analysis using Multiwfn program (A) Scattered RDG plot; (B) Isosurface region; (C) Colour filled ELF plot; (D) Projected ELF plot; (E) Colour filled LOL plot; and (F) Projected LOL plot of 2-bromo-5-methylpyridine

recrystallization needed NCI data. The results of this study produced the Reduced Density Gradient (RDG) map, as is displayed in (Fig. 10A & B). It depends on the electron density and its by-products.

The NCI plot is obtained by plotting the RDG versus the sign for the eigenvalue of the electrons in the Hessian matrix (λ2) multiplied by the value of the density (ρ). The sort of interaction is predicted by the (sign λ2) ρ value. Attraction, Repulsion, and Van der Waals (VDW) links[39] are represented by the values of sign (λ2)ρ, which are sign (λ2)ρ < 0, sign (λ2)ρ > 0, and sign (λ2) ρ ≈ 0. Little red areas at 0.02, 0.03, and 0.04 a.u., as seen in the image, indicated thepresence of weak steric force, while two green shade spikes at 0.015 and 0.02 a.u. indicated the existence of Van der Waals forces on 2BMP. The development of non-covalent areas in 2BMP is shown by the existence of blue colour spikes.

Most research, such as LOL and ELF, only goes so far in exploring topological analysis. A strong likelihood of discovering a pair of electrons on the outermost layer of 2BMP is suggested by the ELF and LOL of Multiwfn software suite. The colour-shaded and relief plots of LOL and ELF are displayed in (Figs 10C-F). The relief chart's condensed or huge peak region indicates the electron location with respect to the relevant atom. The ELF and LOL plots are advanced between 0.0 and 1.0 and 0.0 and 0.8, respectively[40] In nature, the chemical compositions of LOL and ELF are parallel due to circumstances that rely on kinetic energy density. While ELF accounts for the number of electron pairs, LOL provides for the greatest number of localized orbitals that intersect due to the orbital gradient. But if electron localization prevails over electron density, the LOL obtains significant values > 0.5 (i.e., areas below 0.5 indicate delocalized electronic zones).

Hirshfeld analysis

The importance of the interactions for the stability of the crystal lattice has been determined, and their strength and function have been comprehensively investigated, using Hirshfeld surface analysis. The Hirshfeld surfaces of 2BMP are shown in Figure 11A, which shows front and back surface views with d_{norm} range of -1.23 to 0.87 Å. To enable the molecular moiety to be seen, the surfaces are rendered transparent, with each structure having the same orientation. The deep red, considerable circular depressions on the surfaces indicate hydrogen-bonding interactions, reveal how well the data in (Fig. 11B) is summed in these locations. The intermolecular interaction of 2D fingerprint plots[30] are analysed in (Fig. 11C).

The pattern of blue and red triangles on the same area of shape index surfaces actually illustrates the π–π stacking. The big flat region on the curvature surfaces that is indicated by a blue outline illustrates it. The distinctive characteristics are examined in order to determine directional interactions. Figure

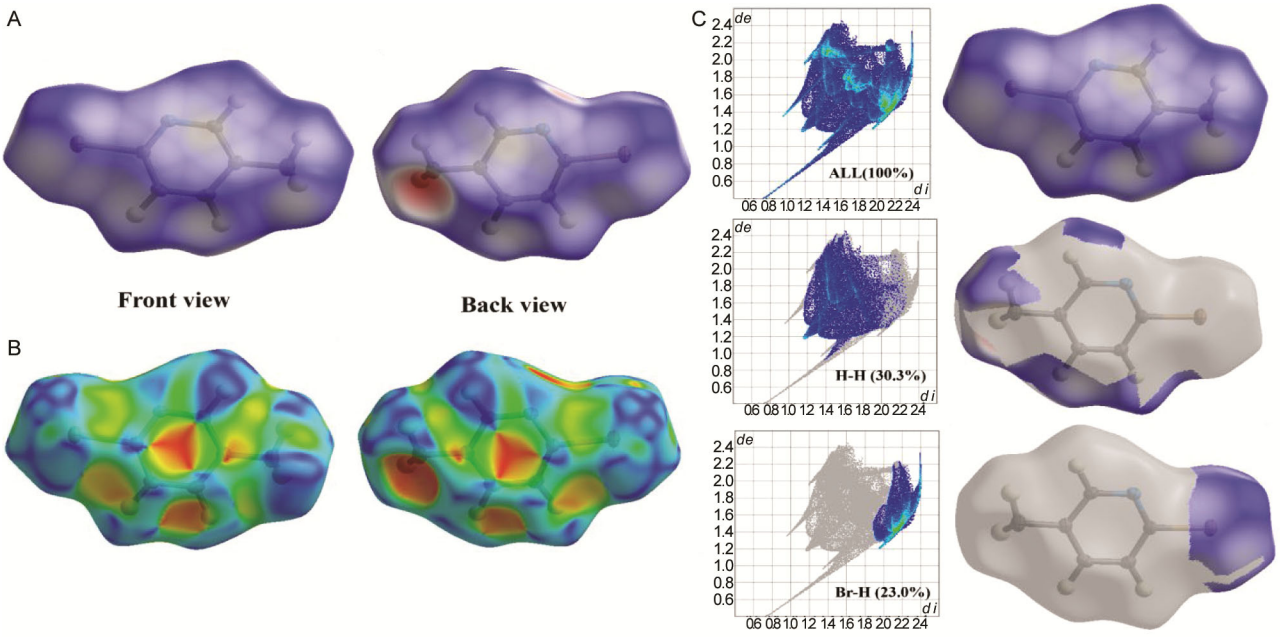

Fig. 11 — (A) d_{norm}front and back view; (B) Shape index; and (C) Fingerprint plot of 2-bromo-5-methylpyridine

11C illustrates this analysis's relative contribution for each contact found in the 2BMP. As noted earlier, H---H connections account for the largest portion of the contribution (30.3%). The fingerprint plot's bottom left (donor) region, which depicts the interaction between acid and water oxygen to create a two-dimensional bond, displays the H---H interactions as a spike. The H-Br interactions are shown as a spike in the lower right section (acceptor) of the fingerprint plot. H-Br interactions make up23% of all Hirshfeld surfaces.

Molecular docking

Pharmacological drug development uses a tool called "molecular docking" to examine the ligand and protein binding sites. Based on previous researc, we have selected few human progesterone and estrogen receptors. The interaction between 2BMP and proteins known to be associated with breast cancer, including the human progesterone (PDB ID: 4OAR) receptor, the epidermal growth factor, the human estrogen (PDB ID: 1ERE) receptor, and the estrogensulfotransferase (PDB ID: 1AQU) receptor, is illustrated in (Fig. 12) of our *in silico* study. When it comes to interactions with the 1AQU protein, Table 10 data show that 2BMP has the highest binding affinity. The binding energy of 1AQU has been found to be -5.4 Kcal mol^{-1} with no hydrogen bond interaction.

Our findings show that 2BMP interacts with the 1ERE receptor of binding energy -5.1 Kcal mol^{-1} by one traditional hydrogen bond, as shown in (Fig. 12). The distances between the residues of ALA A: 350 are 2.99 Å respectively. As seen in Figure 12, 2BMP forms one hydrogen bond with the 4OAR receptor, with LYS A: 822 residues separated by 2.51Å, respectively. The protein 4OAR and the ligand 2BMP have a substantial -5.4 Kcal mol^{-1} affinity for one another. 4OAR has the highest binding energy and contains the hydrogen bond with the least distance. The 2BMP ligand consequently binds with the proteins associated with breast cancer and has the potential to suppress its activity.

ADMET analysis

The study shows the absorption and metabolism properties of 2BMP in (Table 11). There is more Caco-2 permeability present if the log Papp value recorded by the pkCSM server is greater than 0.90. In order to absorb food and medications, the human intestine is necessary. It is considered that compounds have poor human intestinal absorption (HIA) when

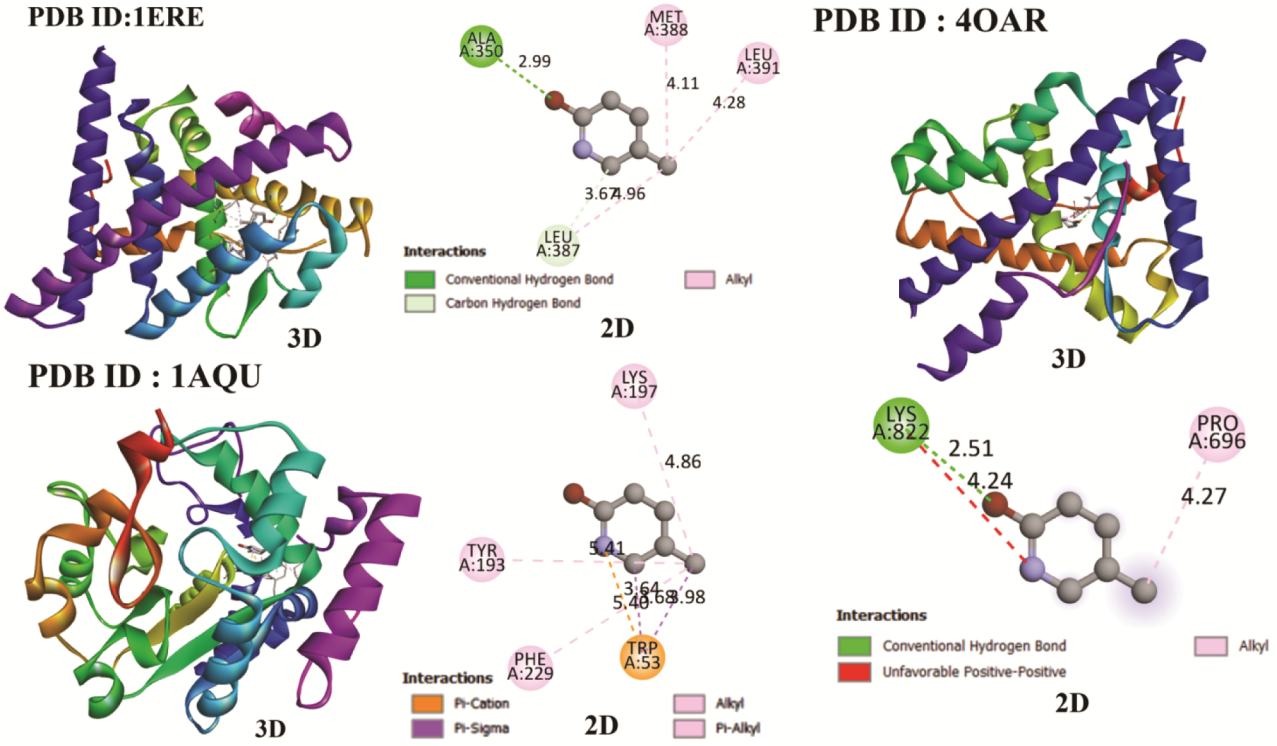

Fig. 12 — Molecular Docking of 3D and 2D interaction with H-Bond donor-acceptor colour grade of 2-bromo-5-methylpyridine with PDB ID: 1ERE, 1AQU and 4OAR target proteins

Table 10 — Comparison of binding energies of 2-bromo-5-methylpyridine

S. No	Protein	Binding Energy (Kcal/mol)	Interacted Residues	Ligand and Protein atom involved in H-bonding
1.	1ERE	5.1	ALA A: 350, MET A:388, LEU A :391, LEU A :387	ALA A : 350
2.	1AQU	-5.4	LYS A: 197, TYR A:193, PHE A: 229, TRP A:53	-
3.	4OAR	-5.4	LYS A: 822, PRO A: 696	LYS A: 822

Table 11 — ADMET profile of 2-bromo-5-methylpyridine

ADMET prediction		Value	ADMET prediction		Value	Pharmacokinetic properties		Value
Absorption	CaCo-2 permeability (log Papp in 10^{-6} cm/s)	1.7	Excretion	Total Clearance (log mL/min/kg)	-0.014	Physiochemical properties	Molecular weight (g/mol)	172.02
							No. of Hydrogen bond acceptors	1
							No. of Hydrogen bond donors	0
							Fraction Csp 3	0.17
	Intestinal absorption (human) (%)	96.635						
	Skin Permeability (log Kp)	-2.184		Renal OCT2 substrate	No	Water Solubility	ESOL	-2.97
	P-glycoprotein substrate	Yes		Renal OCT2 substrate			ALI	-2.30
	P-glycoprotein I inhibitor	No					SILICOS-IT	-3.26
	P-glycoprotein II inhibitor	No	Toxicity	AMES toxicity test	No	Lipophilicity	iLOGP	1.93
Distribution	VDss (human) (log L/kg)	-0.082		Max. tolerated dose (human)	1.078		XLOGP3	2.39
	Fraction unbound (human) (Fu)	0.559		(log mg/kg/day)			WLOGP	2.15
	BBB permeability (log BB)	-0.139		hERG I inhibitor	No		MLOGP	1.58
							SILICOS-IT	2.54
	CNS permeability (log PS)	-2.541		hERG II inhibitor	No	Drug Likeness	Lipinski	Yes, 0, violation
Metabolism	CYP2D6 substrate	No		Oral Rat Acute Toxicity (LD50) (mol/kg)	2.442			
	CYP3A4 substrate	No		Oral Rat Chronic	1.792			
	CYP1A2 inhibitor	No		Toxicity (LOAEL) (log mg/kg_bw/day)			Veber	Yes
	CYP2C19 inhibitor	No		Hepatotoxicity	No			
	CYP2C9 inhibitor	No		Skin Sensitisation	Yes		Ghose	No
	CYP2D6 inhibitor	No		T.Pyriformis**toxicity** (log ug/L)	0.12		Egan	Yes
	CYP3A4 inhibitor	No		Minnow toxicity (log mM)	1.327		Bioavailability Score	0.55

their absorption level is less than 30%[41]. In the human gut, 2BMP absorbs 96.635% of its contents. When given orally, a higher HIA suggests that the drug may be more absorbed from the digestive tract. The most challenging barrier in topical drug development is breaking through the skin's protective layer. Various *in silico* techniques are used to predict the degree of skin penetration of the 2BMP. The skin permeability (logKp) of -2.184, as reported by the pkCSM server data, suggests that 2BMP has superior dermal permeability. The hypothetical volume of distribution, or VDss, is the whole dosage of a drug that would be distributed uniformly to provide a concentration similar to blood plasma. Increased VDss indicates a wider distribution of the medication in tissue compared to plasma. 2BMP was discovered with a VDss (log L/kg) of -0.082, indicating a substantial volume of dispersion.

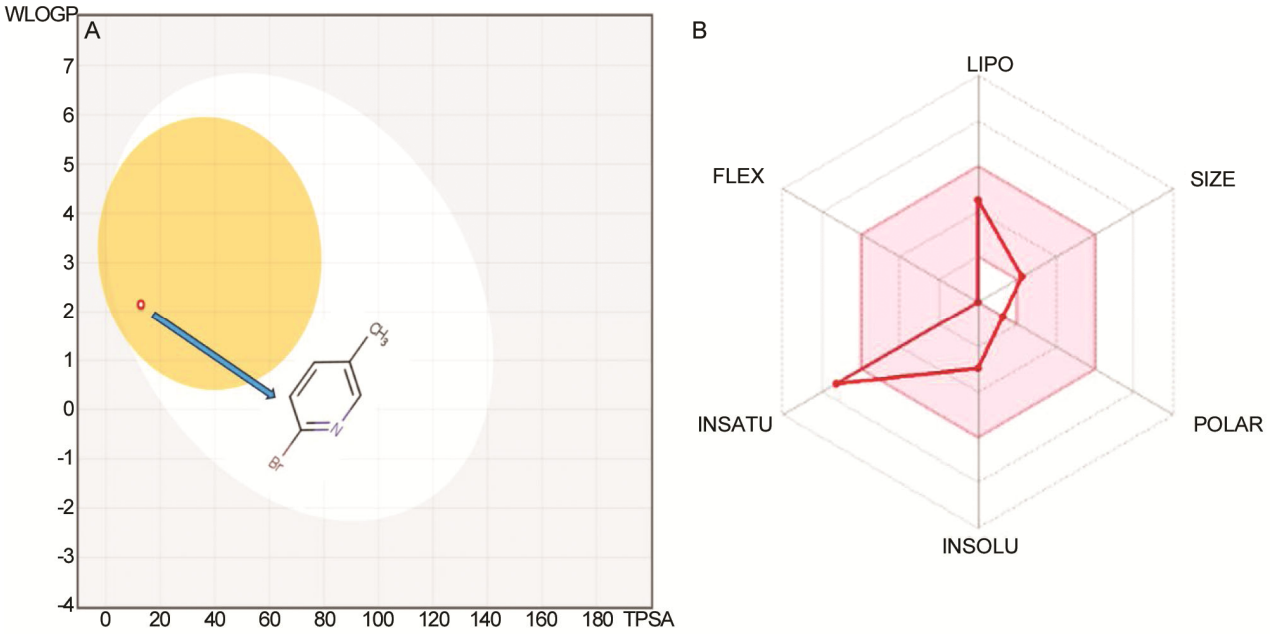

Fig. 13 — (A) BOILED-Egg plot; and (B) Radar plot of 2-bromo-5-methylpyridine

It indicates that the brain can be shielded from dangerous drugs by the permeable Blood-Brain Barrier (BBB). A blood-brain barrier perforation rate of more than 0.3 suggests that the chemical may be easily able to cross it, while a logBB of -1 indicates that the molecule is poorly distributed to the brain. LogBB of -0.139 on the pkCSM server indicates that 2BMP is significantly disseminated to the brain. Another straight assessment that is performed via in situ brain insertion with the medication administered right away into the carotid artery is CNS permeability (logPS). According to the pkCSM prediction method, compounds with logPS> -2 are thought to be able to enter the central nervous system, whereas compounds with logPS<-3 are thought to be unable to do so. According to research, 2BMP has a logPS value of -2.541, which means it can enter the central nervous system. Using 2BMP as a renal OCT2 substrate, the pkCSM server reports a total clearance rate of -0.014. The oral 2BMP treatment in rats was shown to have acute and chronic toxicity limits of 2.442 mol/kg (LD50) and 1.792 log mg/kg bw/day (LOAEL). No inhibition of hERG I or II is observed by pkCSM server for 2BMP. P-gP is believed to play a part in the BOILED Egg Model of 2BMP. It is present in numerous excretory systems, such as the hepatic, intestinal, and renal ones. P-gP activation and inhibition are essential phases in the metabolism of drugs.

The efficaciousness, lipophilicity, solubility, and the Boiled egg model of lead compound 2BMP are assessed by SwissADME,[42] a free online program; the outcomes are presented in (Table 11). In this study, the yellow section of the yolk is said to represent brain penetration, and the white part, or albumin part, stands for gastrointestinal absorption. Figure 13A shows that the drug component appears inside the yolk region of 2BMP BOILED Egg model. This illustrates the drug's capacity to penetrate the BBB. The lone instance of the Ghose rule being broken occurred with the 2BMP, whose molecular weight was 172.02 g/mol. The Fraction of sp3 carbon atoms can be used to describe the aliphatic degree and forecast the solubility of a medicinal molecule. According to certain theories, the therapeutic success rate of a given chemical increases with increasing saturation. The pharmacological molecule under research was found to have a Fraction Csp3 of 0.90, indicating a high degree of saturation, according to the study. Figure 13B displays the radar plot that was obtained. The lipophilicity of iLOGP, XLOGP3, WLOGP, MLOGP, and SILICOS-IT wasestimated to be 1.93, 2.39, 2.15, 1.58, and 2.54, respectively. It was projected that the decanal water solubility for ESOL, ALI, and SILICOS-IT would be -2.97, -2.30, and -3.26, respectively. The water solubility values obtained indicate a range from somewhat soluble to highly soluble. The expected pharmacokinetic properties confirm that the 2BMP is sufficiently safe to be considered as a viable therapeutic.

Conclusion

Applying the DFT-B3LYP approach with the conventional 6-311++G(d,p) basis set calculations has yielded the optimal geometries, harmonic vibrational wave numbers, and intensities of vibrational bands of 2BMP. The computation level was found to be more consistent with experimental findings. Evidence supporting the frequency assignment is provided by the PED calculation. It is observed thatUV-Vis spectral values are compared with the electronic characteristics. It was used to find the NMR chemical shifts for ^{1}H and ^{13}C, which are more consistent with the experiment's findings. Reduced density gradient analysis was used to evaluate the weak interactions of 2BMP, while the localized orbital locator and electron localization function were used to evaluate the molecule's structure. Atom-to-atom interactions in crystal packing modes are characterized by their kind and intensity using two-dimensional finger maps and the Hirshfeld surface analysis. It has been found that 2BMP binds most strongly to the breast cancer proteins 1ERE, 1AQU, and 4OAR, with the highest affinity energy values of -5.1, -5.4, and -5.4 $Kcalmol^{-1}$, respectively. Their binding affinity is comparable to that of the common drug anastrozole (-5.9 $Kcal\ mol^{-1}$). Ultimately, the physicochemical and ADMET properties supported the drug-like characteristics of 2BMP, demonstrating the molecule's safety and non-violation of any Lipinski rules.

Acknowledgement

The author expresses gratitude to Kalasalingam Academy of Research and Education's administration for their support and for granting the opportunity to conduct this study.

Conflict of interest

All authors declare no conflict of interest.

References

1 Islam MB, Islam MI, Nath N, Emran T Bin, Rahman MR & Sharma R, Recent Advances in Pyridine Scaffold: Focus on Chemistry, Synthesis, and Antibacterial Activities. *Biomed Res Int,* (2023).

2 Allaka TR & Katari NK, Synthesis of pyridine derivatives for diverse biological activity profiles: a review. *Recent Dev Synth Appl Pyridines,*(2023) 605

3 Mohamed EA, Ismail NSM, Hagras M & Refaat H, Medicinal attributes of pyridine scaffold as anticancer targeting agents. *Futur J Pharm Sci,* 7(2021) 1.

4 Aliabadi A, Motieiyan E, Hosseinabadi F, Ghadermazi M& Abdolmaleki S, One-pot synthesis, crystallographic characterization, evaluation as *in vitro* antibacterial and cytotoxic agents of two mercury (II) complexes containing pyridine dicarboxylic acid derivatives. *J Mol Struct,* 1226 (2021) 129405.

5 Chen YJ, Huang SM, Tai MC, Chen JT, Lee AR & Huang RY, The anti-fibrotic and anti-inflammatory effects of 2, 4-diamino-5-(1-hydroxynaphthalen-2-yl)-5H-chromeno [2, 3-b] pyriine-3-carbonitrile in corneal fibroblasts. *Pharmacol Report,* 72 (2020) 25.

6 Ali EMH, Abdel-Maksoud MS, Hassan RM, Mersal KI, Ammar UM & Se-In C, Design, synthesis and anti-inflammatory activity of imidazol-5-yl pyridine derivatives as p38α/MAPK14 inhibitor. *Bioorg Med Chem,* 31 (2021) 115969.

7 Bass AK, Abdelhafez E, El-Zoghbi M, Mohamed MFA, Badr M & Abuo-Rahma GEDAA, 3-Cyano-2-oxa-pyridines: a promising template for diverse pharmacological activities. *J Adv Biomed Pharm Sci,* 4 (2021) 81.

8 Hammoudi NEH, Benguerba Y, Attoui A, Hognon C, Lemaoui T & Sobhi W, *In silico* drug discovery of IKK-β inhibitors from 2-amino-3-cyano-4-alkyl-6-(2-hydroxyphenyl) pyridine derivatives based on QSAR, docking, molecular dynamics and drug-likeness evaluation studies, *J Biomol Struct Dyn,* 40 (2022) 886.

9 Sugiyama S, Akiyama T, Taoda Y, Iwaki T, Matsuoka E & Akihisa E, Discovery of novel HIV-1 integrase-LEDGF/p75 allosteric inhibitors based on a pyridine scaffold forming an intramolecular hydrogen bond. *Bioorg Med Chem Lett,* 33 (2021)127742.

10 Aarthi KV, Rajagopal H, Muthu S, Jayanthi V & Girija R, Quantum chemical calculations, spectroscopic investigation and molecular docking analysis of 4-chloro-N-methylpyridine-2-carboxamide. *J Mol Struct,* 1210 (2020) 128053.

11 Lefi N, Kazachenko AS, Raja M, Issaoui N & Kazachenko AS, Molecular Structure, Spectral Analysis, Molecular Docking and Physicochemical Studies of 3-Bromo-2-hydroxypyridine Monomer and Dimer as Bromodomain Inhibitors. *Molecules,* 28 (2023) 6.

12 Penny LK & Wallace HM. The challenges for cancer chemoprevention. *Chem Soc Rev*, 44 (2015) 8836.

13 Premkumar S, Jawahar A, Mathavan T, Kumara Dhas M, Sathe VG & Milton Franklin Benial A, DFT calculation and vibrational spectroscopic studies of 2-(tert-butoxycarbonyl (Boc) -amino)-5-bromopyridine. *Spectrochim Acta - Part AMol Biomol Spectrosc*, 129 (2014) 83.

14 Ramuthai M, Jeyavijayan S, Premkumar R, Uma Priya M & Jayram ND, Structure, Spectroscopic Investigation, Molecular Docking and *in vitro* Cytotoxicity Studies on 4,7-dihydroxycoumarin: A Breast Cancer Drug. *J Comput Biophys Chem,* 21 (2022) 219.

15 Frisch MJ, Trucks GW, Schlegel HB, Scuseria GE, Robb MA, Cheeseman JR, Scalmani G,Barone V, Petersson GA, Nakatsuji H,Li X, Caricato M, Marenich A, Bloino J, Janesko BG, Gomperts R, Mennucci B, Hratchian HP, Ortiz JV, Izmaylov AF, Sonnenberg JL, Williams-Young D, Ding F, Lipparini F, Egidi F, Goings J, Peng B, Petrone A, Henderson T, Ranasinghe D, Zakrzewski VG, Gao J, Rega N, Zheng G, Liang W, Hada M, Ehara M, Toyota K, Fukuda R, Hasegawa J, Ishida M, Nakajima T, Honda Y, Kitao O, Nakai H, Vreven T, Throssell K, Jr. Montgomery JA, Peralta JE, Ogliaro F, Bearpark M, Heyd JJ, Brothers E, Kudin KN, Staroverov VN, Keith T, Kobayashi R, Normand J, Raghavachari K, Rendell A, Burant JC, Iyengar SS, Tomasi J, Cossi M, Millam JM, Klene M, Adamo C, Cammi R,

Ochterski JW, Martin RL, Morokuma K, Farkas O, Foresman JB & Fox DJ, Gaussian, Inc., Wallingford CT, 2016. Gaussian 09. 2013 Gaussian 09, Revision A.02, Gaussian, Inc., Wallingford CT.

16 Jamróz MH, Vibrational energy distribution analysis (VEDA): Scopes and limitations. *Spectrochim Acta - Part A Mol Biomol Spectrosc,* 114 (2013) 220.

17 Becke AD, Thermo chemistry Density-Functional III. The Role of Exact Exchange. *J Chem Phys,* 98 (1993) 5648.

18 Rauhut G & Pulay P, Transferable scaling factors for density functional derived vibrational force fields. *J Phys Chem,* 99 (1995) 3093.

19 Kunjumol VS, Jeyavijayan S, Sumathi S & Karthik N, Spectroscopic, computational, cytotoxicity, and docking studies of 6-bromobenzimidazole as anti-breast cancer agent. *J Mol Recognit*, 37 (2024) e3074.

20 O'boyle NM, Tenderholt AL & Langner KM, Cclib: a library for package-independent computational chemistry algorithms. *J Comput Chem*, 29 (2008) 839.

21 Lu T & Chen F, Multiwfn: A multifunctional wavefunction analyzer. *J Comput Chem*, 33 (2012) 580.

22 Seeliger D & de Groot BL, Ligand docking and binding site analysis with PyMOL and Autodock/Vina. *J Comput Aided Mol Des*, 24 (2010) 417.

23 Trott O & Olson AJ, AutoDock Vina: improving the speed and accuracy of docking with a new scoring function, efficient optimization, and multithreading. *J Comput Chem*, 31 (2010) 455.

24 Mohan UP, Kunjiappan S, Tirupathi PBP& Arunachalam S, Adriamycin inhibits glycolysis through downregulation of key enzymes in *Saccharomyces cerevisiae*. *3 Biotech*, 11 (2021) 1.

25 Srivastava R, Gupta SK, Naaz F, Sen Gupta PS, Yadav M & Singh VK. Alkylated benzimidazoles: Design, synthesis, docking, DFT analysis, ADMET property, molecular dynamics and activity against HIV and YFV. *Comput Biol Chem,* 89 (2020) 107400.

26 Daina A, Michielin O & Zoete V, SwissADME: a free web tool to evaluate pharmacokinetics, drug-likeness and medicinal chemistry friendliness of small molecules. *Sci Rep*, 7 (2017) 42717.

27 Roy M, Golen JA, Manke DR. 2-Bromo-5-methylpyridine. IUCrData. 2016;1(1).

28 Sumathi S, Jeyavijayan S, Karthik N, Karthikeyan A, Murugan P & Kunjumol VS, Molecular Structure, Spectroscopy, Molecular Docking and ADMET Studies of 2,5-Dimethylbenzaldehyde Semicarbazone as Potent Breast Cancer Agent. *Asian J Chem,* 36 (2024)1.

29 Kunjumol VS, Jeyavijayan S, Karthik N & Sumathi S, Spectroscopic, Computational, Docking and Cytotoxicity Studies on 2-(2-Chlorophenyl) benzimidazole as a Potent Anti-breast Cancer Agent. *Indian J Pure Appl Phys,* 62 (2024) 576.

30 Kumar JS, Karthik N, Sumathi S, Jyothi NS, Saranya S & Jeyavijayan S, DFT Computation, Spectroscopic, Hirshfeld Surface, Docking and Topological Analysis on 2,2,5-Trimethyl-1,3-Dioxane-5-Carboxylic Acid as Potent Anti-Cancer Agent. *Int J Quantum Chem*, 124 (2024) 1.

31 Sumathi S, Jeyavijayan S & Karthik N, Spectroscopic Investigations , Quantum Chemical , Molecular Docking and Drug Likeness Studies of 3-Fluorobenzamide. *J Sci Ind Res,* 83 (2024) 1373.

32 Saha SK, Dutta A, Ghosh P, Sukul D & Banerjee P, Adsorption and corrosion inhibition effect of Schiff base molecules on the mild steel surface in 1 M HCl medium: a combined experimental and theoretical approach. *Phys Chem Chem Phys,* 17 (2015)5679.

33 Domingo LR, Aurell MJ, Pérez P & Contreras R, Quantitative characterization of the global electrophilicity power of common diene/dienophile pairs in Diels–Alder reactions. *Tetrahedron,* 58 (2002) 4417.

34 Kunjumol VS, Jeyavijayan S, Karthik N & Sumathi S, Spectroscopic, computational, docking, and cytotoxicity investigations of 5-chloro-2-mercaptobenzimidazole as an anti-breast cancer medication. *Spectrosc Lett,* (2024) 1.

35 Abraham CS, Prasana JC, Muthu S, Rizwana B F & Raja M, Quantum computational studies, spectroscopic (FT-IR, FT-Raman and UV–Vis) profiling, natural hybrid orbital and molecular docking analysis on 2,4 Dibromoaniline. *J Mol Struct* 1160 (2018) 393.

36 Ayers PW & Parr RG, Variational principles for describing chemical reactions: the Fukui function and chemical hardness revisited. *J Am Chem Soc,* 122 (2000) 2010.

37 Morell C, Grand A &Toro-Labbé A, New Dual Descriptor for Chemical Reactivity. *J Phys Chem A*, 109 (2005) 205.

38 Johnson ER, Keinan S, Mori-Sánchez P, Contreras-García J, Cohen AJ & Yang W, Revealing noncovalent interactions. *J Am Chem Soc,* 132(2010) 6498.

39 Saleh G, Gatti C & Presti L Lo, Non-covalent interaction via the reduced density gradient: Independent atom model vs experimental multipolar electron densities. *Comput Theor Chem,* 998(2012) 148.

40 Chandran K, Zochedh A, Sultan AB & Kathiresan T, Observations into quantum simulation, spectroscopy, electronic properties, pharmacokinetics and molecular docking analysis of lawsone against breast cancer. *J Mol Struct,* 1293 (2023) 136280.

41 Sukumaran S, Zochedh A, Viswanathan TM, Sultan AB & Kathiresan T, Theoretical investigation of 5-fluorouracil and tamoxifen complex–structural, spectrum, DFT, ADMET and docking simulation. *Polycycl Aromat Compd,* 43 (2023) 9443.

42 Azzam KAL, SwissADME and pkCSM webservers predictors: An integrated online platform for accurate and comprehensive predictions for *in silico* ADME/T properties of artemisinin and its derivatives. *Kompleks Ispolz Miner Syra= Complex use Miner Resour,* 325 (2023) 14.